Geophysical observations and structural models of two shallow caves in gypsum/anhydrite-bearing rocks in Germany

GEORG KAUFMANN* & DOUCHKO ROMANOV

Institute of Geological Sciences, Geophysics Section, Freie Universität Berlin, Malteserstrasse 74-100, Haus D, 12249 Berlin, Germany

**Correspondence: georg.kaufmann@fu-berlin.de*

Abstract: The development of subsurface voids and cavities in soluble rocks is controlled by the hydrological and chemical processes in the host rock. Water (enriched with carbon dioxide) percolates through fractures and bedding partings of the host rock and removes material from the rock surface. As this enlargement is a highly heterogeneous process, only some fractures and bedding partings become significantly enlarged, evolving towards larger voids and caves. The size of the enlarged voids, often reaching the metre scale, can result in mechanically unstable structures, which, when close to the surface, are prone to collapse and thus are a hazard to infrastructure. We explored two caves in the anhydrite host rock of the Permian Zechstein sequences in northern Germany using geophysical measurements: the Kalkberghöhle close to Bad Segeberg (Hamburg region) and the Jettenhöhle close to Osterode (Harz region). Based on the results of gravity and electrical measurements, we were able to identify the cave voids and to characterize the local geological setting. Using these indirect geophysical observations, we deduced a structural model for both cave sites by numerical modelling. Our structural models were successfully calibrated against the Bouguer gravity data.

A wide variety of soluble host rocks can be found in different parts of Germany (Fig. 1). The soluble host rocks range from Devonian limestones in the west to Jurassic limestones in the south. The evaporitic sequences of the Permian Zechstein period characterize the landscape in central and northern Germany, either as outcrops exposed through the tectonic uplift of the southern Harz Mountains, or buried at *c.* 4–6 km depth beneath the entire northern German basin. In the latter area, localized salt diapirism has caused the uplift of soluble rocks, bringing them closer to the present day surface.

The soluble host rocks can be dissolved by water (enriched with carbon dioxide) percolating through the rock, removing material from fractures and bedding planes and later enlarging these flow paths (Ford & Williams 2007). With time, the permeability in the host rock increases substantially at the local scale and creates the larger voids and caves typical of subsurface karst features in the soluble host rock (Palmer 2007; Gutiérrez 2010; De Waele *et al.* 2011; Gutiérrez *et al.* 2014).

Geophysical methods can be used to detect these subsurface voids using indirect measurements. Most of these geophysical methods distinguish between the material properties (e.g. density, electrical resistivity and electrical permittivity) of the void and its infill and the significantly different material properties of the surrounding host rock. This contrast in material properties can be detected using specific geophysical techniques (e.g. Butler 1984; El-Qady *et al.* 2005; Dobecki & Upchurch 2006; Bechtel *et al.* 2007; Mochales *et al.* 2008; Parise & Lollino 2011; Margiotta *et al.* 2012, 2016; Carbonel *et al.* 2013, 2014; Kaufmann 2014; Kaufmann & Romanov 2016).

Different geophysical methods provide complementary information about the subsurface voids.

(1) Air- and water-filled voids have a much lower density (0 and 1000 kg m^{-3} for air and water) than the host rock (2200 and 2900 kg m^{-3} for gypsum and anhydrite, respectively). The sediment infill of a cavity also often has a lower density than the host rock. Gravity measurements can be used to detect the density differences between the low densities of the voids and the higher densities of the host rock and thus the likely location of subsurface voids.

(2) The electrical resistivity of the host rock is mainly determined by the fluids circulating in the void spaces of the rock. Thus the bulk electrical resistivity of the rock is mainly determined by the amount of fractures and their interconnections and infill. Although limestone, dolomite and anhydrite have a high resistivity (*c.* 1000–2000 Ω m; Telford *et al.* 2012), gypsum is often highly fractured close to the surface and provides interconnected pathways for circulating water and

From: Parise, M., Gabrovsek, F., Kaufmann, G. & Ravbar, N. (eds) 2018. *Advances in Karst Research: Theory, Fieldwork and Applications*. Geological Society, London, Special Publications, **466**, 341–357.
First published online December 6, 2017, https://doi.org/10.1144/SP466.13

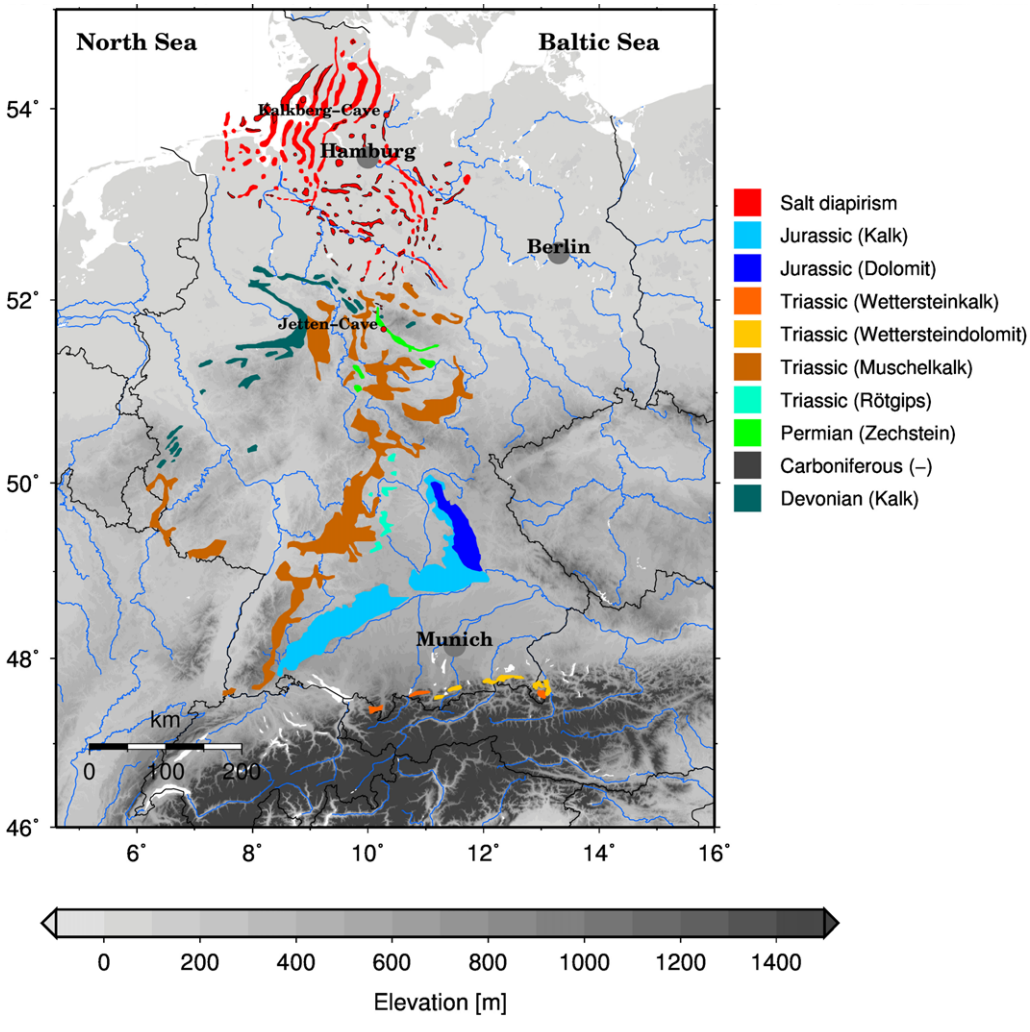

Fig. 1. Map of Germany showing outcrops of soluble rocks by geological epoch and the occurrence of salt diapirs in the northern German basin. The locations of major cities and the two studied caves are shown.

thus shows a lower resistivity. Cavities in the host rock represent either highly resistive areas if they are air-filled, or a lower resistivity if they are water-filled. A sediment infill can be highly resistive if it is dry or have a low resistivity if it is wet. Thus electrical resistivity imaging (ERI) mainly provides information about the amount of water in the subsurface.

(3) Locations where groundwater is accessible – such as sinks, resurgences, streams and lakes – in a cave can be sampled directly with electrical conductivity measurements. These measurements only probe the water component of the host rock and thus provide a different picture of the distribution of electrical resistivity from ERI. When combined with ERI, electrical conductivity measurements can distinguish the host rock matrix from water-filled fractures and bedding partings.

(4) Groundwater percolating through the unsaturated zone can drag excess electrical charges with it. These charges will induce an electrical potential difference, which can be mapped using the self-potential method. The groundwater-induced self-potential is often in the range of a few tens of millivolts.

(5) Ground-penetrating radar can reveal the subsurface structure from the reflection of electromagnetic waves.

The application of different geophysical methods provides a broad indirect picture of the voids in soluble host rocks and can help to unravel the strong preferential distribution of voids and cavities enlarged by dissolution in the subsurface. These indirect observations can then be used to infer the void geometry by forward and inverse modelling of the geophysical measurements.

We present here the results from geophysical surveys above two caves in Permian Zechstein rocks in Germany (Fig. 1). The Kalkberghöhle cave is located in the Hauptanhydrit caprock of a salt diapir in northern Germany, whereas the Jettenhöhle cave developed in the Hauptanhydrit formation exposed along the southern Harz Mountains in Germany. We aimed to identify both cave voids and, in some areas, the local stratigraphy from the geophysical signatures (gravity, ERI and self-potential measurements). We present structural models of the subsurface based on our geophysical results.

Geophysical methods

This section introduces the geophysical methods used to detect the subsurface structures in the areas of interest.

Gravity

We carried out the gravimetric survey using Lacoste-Romberg type D gravimeters with a precision estimated to be better than 0.03 mGal from repeated readings. The survey station coordinates were recorded with a hand-held global positioning system monitor to about 1 m accuracy, whereas the elevations were determined to 3 cm accuracy by levelling with a levelling rod. The raw data were processed with GRAViMAG software developed at the Geophysics Department, Freie Universität Berlin to derive the Bouguer gravity, Δg_b (mGal). We used four processing steps to derive the Bouguer gravity data from the raw measurements: (1) repeated base station measurements roughly every 2–3 h to monitor instrument drift; (2) correction of Earth tides based on the software package Eterna (Wenzel 1996); (3) linking the relative gravity measurements into the regional gravity network through a known station with absolute gravity; and (4) using latitude, free-air and Bouguer corrections, including a topographic Bouguer correction (where needed) derived from either the Shuttle Radar Topography Mission digital elevation model (Jarvis *et al.* 2008) or a local digital elevation model when a higher accuracy was needed. The densities ranged from 0 kg m^{-3} for the air-filled cave passages to *c.* 1500 kg m^{-3} for the cave sediments, and 2200 and 2900 kg m^{-3} for gypsum and anhydrite, respectively, as the host rock (e.g. Telford *et al.* 2012).

Electrical resistivity imaging

ERI was carried out along the profiles with a Geo-Tom MK8E1000 instrument and 25–75 steel electrodes, mostly in the Wenner and Schlumberger set-up. We also tested dipole–dipole configurations, often better suited to detecting lateral contrasts in electrical resistivity, but due to the poor signal-to-noise ratio of this set-up we decided not to use these measurements. The raw data were processed with the Res2DInv software package (Loke & Barker 1995, 1996), applying robust inversion methods, to derive the electrical resistivity, ρ_e (Ω m). Poor datum points were removed with the help of the software prior to inversion by identifying the gross outliers along each horizontal pseudo-depth section. Coordinates for the electrodes were taken with a hand-held global positioning system monitor and the elevation either from levelling or from the digital elevation map. Inversions of the profiles were carried out, including the topographic elevation. The electrical resistivity of the gypsum and anhydrite was *c.* 400–1000 Ω m, depending on the infill of fissures, whereas the air-filled cave voids had a resistivity >4000 Ω m (e.g. Telford *et al.* 2012).

Electrical conductivity

A hand-held electrical conductivity meter (ADWA Instruments) was used to measure the electrical conductivity, σ_e (S m^{-1}), in open water bodies (cave lakes, creeks and springs). The electrical conductivity values were calibrated to a temperature of 25°C.

Self-potential

Self-potential surveying was carried out with laboratory-made non-polarizable copper–copper sulphate electrodes and a Voltcraft multimeter. One electrode served as the base from which the potential difference, ΔU (mV), was mapped across the survey area. The base electrode was located outside the sampling profiles. A hole was dug for all the electrodes to achieve good coupling conditions between the electrodes and the soil. Measurements were carried out within a time frame of 2 h and therefore the diurnal variation was small. We expected streaming potentials in the range of tens of millivolts from subsurface water channelled into the wider fractures opened by dissolution, thus inducing preferential groundwater flow towards a base level.

Cave sites

This section presents the results of the geophysical surveys above the two cave sites (Fig. 1). Both sites are located in Hauptanhydrit, the anhydrite

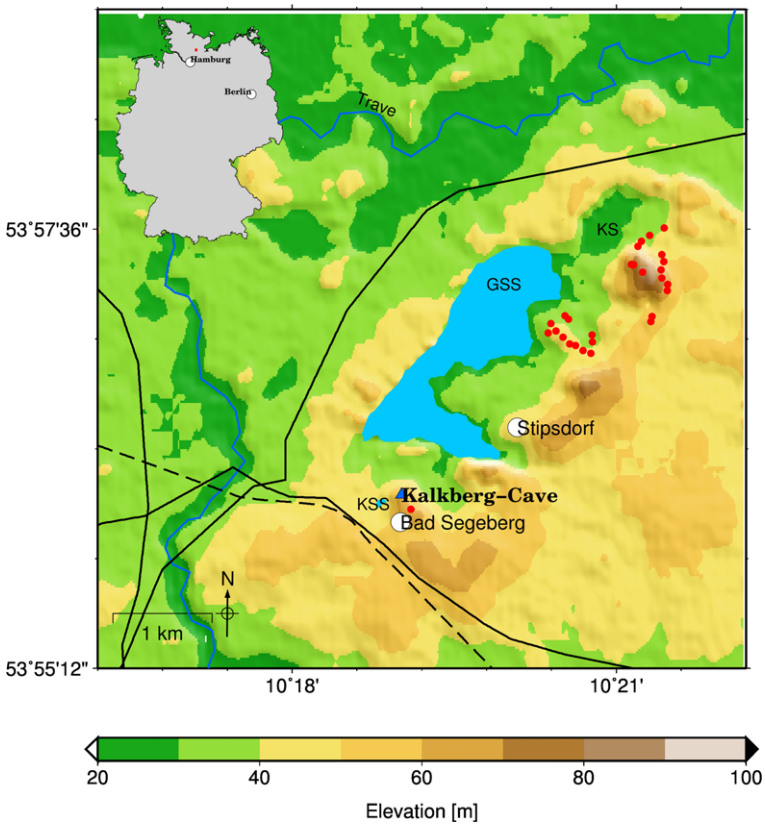

Fig. 2. Map of Bad Segeberg showing the study site (red square) and the Kalkberg cave (blue triangle), cities (white dots), sinkholes (red circles), rivers (light blue lines), roads (black solid lines) and railways (black dashed lines). GSS, Grosser Segeberger See; KSS, Kleiner Segeberger See; KS, Klüthsee. The inset shows the location (red square, north of Hamburg) of the figure within Germany.

part of the z3 (Leine) sequence of the Permian Zechstein deposits in Germany.

Kalkberghöhle

The Kalkberghöhle is located close to the city of Bad Segeberg (Fig. 2) in the northern German basin, with elevations *c.* 10–40 m above sea-level (a.s.l.). Salt diapirism since the Keuper period has caused uplift of the deeply buried soluble Zechstein rocks closer to the surface, with the Segeberg salt diapir responsible for exposing the Hauptanhydrit along the north-trending axis of the diapir (e.g. Kardel *et al.* 2009; Ipsen & Mucke 2011). On the surface, the lakes Grosser Segeberger See (28.9 m a.s.l.), Kleiner Segeberger See (37.9 m a.s.l.) and Klüthsee (*c.* 28 m a.s.l.) mark the axis of the salt diapir as subrosion depressions. Three major fault zones are mapped perpendicular to the long axis of the salt diapir and the two northern fault zones are lined by a series of sinkholes (Ross 1993). The Kalkberg, a hill with a former height of 114 m a.s.l., was topped by a castle in early Medieval times (e.g. Sparr 1997; Ipsen & Mucke 2011). Its name, including the German word Kalk (limestone), is misleading because of the exposed anhydrite, but stems from the Medieval mining use of Kalk as a term to describe soluble rocks.

Drinking water for the Medieval castle was recovered from a well, with its opening originally at *c.* 110 m a.s.l. After the castle had been destroyed, open-pit mining of the anhydrite and its gypsum shell substantially lowered height of the hill, with its highest peak today at 90 m a.s.l. The main quarry has been re-cultivated and rebuilt to host an open-air theatre (Fig. 3). In 1807, the former well was excavated again and a drillhole was lowered into the Hauptanhydrit from the bottom of the well at 26.4 m a.s.l. in hope of finding salt (Fig. 3d). The drillhole ended at −62 m a.s.l., still within the Hauptanhydrit. Two further drillholes along the eastern shores of the Grosser Segeberger See then reached

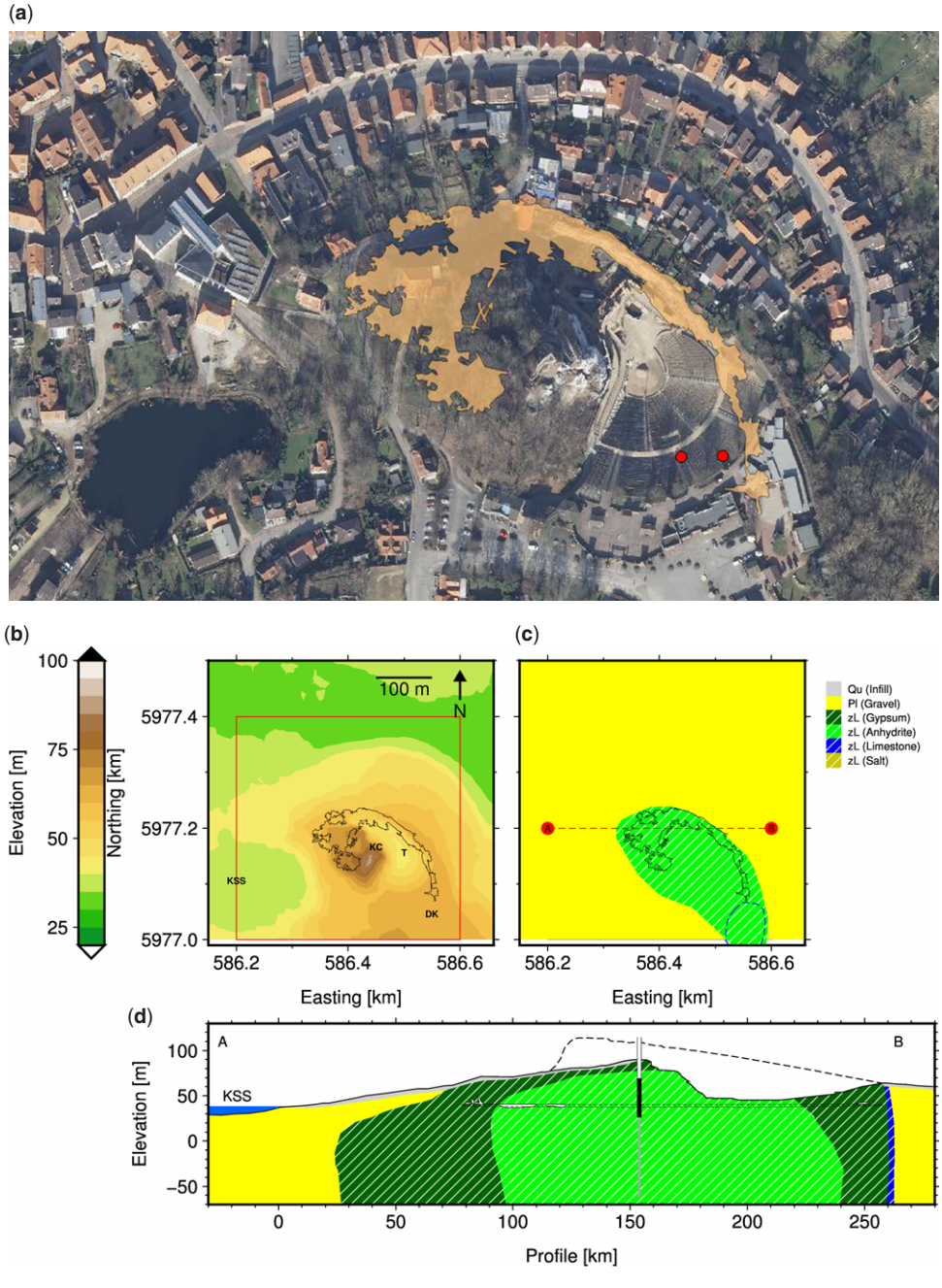

Fig. 3. Kalkberghöhle, Bad Segeberg, Schleswig-Holstein, Germany. (**a**) Map of the Kalkberghöhle cave superimposed onto the digital ortho-photograph of the area. The two red dots mark the former mining shafts. (**b**) Map view of the study area. KC, Kalkberghöhle cave; KSS, Kleiner Segeberger See; T, open-air theatre; DK, Damloser Kuhle sinkhole. The survey area is shown by the red rectangle. (**c**) Geological map showing the lithological units. The location of the geological cross-section in part (d) is marked by the red dashed line. (**d**) Geological cross-section along the profile shown in part (c). The former land surface is shown as a dashed line, the well removed in part by mining is shown in white and existing part of the well is shown in black. The drillholes lowered from the bottom of the well are shown in grey. The blue area is the KSS. The cave is shown as a white area, with the cave level indicated by dashed lines.

the Stassfurt salt at about 103 and 149 m depth, respectively. With the idea of starting salt mining, two shafts were lowered in the main quarry (now the open-air theatre), reaching depths of 88 and 116 m. However, both shafts flooded due to unmanageable water inflow from the surrounding rock (Sparr 1997).

A substantial maze cave, the Kalkberghöhle, with about 2 km of passages, has been explored beneath the remnants of the Kalkberg (Fricke 1990). Detailed geological mapping of the cave (Ross 1990) revealed that although the central parts of the Kalkberghöhle are located in the Hauptanhydrit and thus fairly stable, the outer parts of the cave (in the west and SE) are developed in the gypsum part and are fairly unstable and prone to roof collapse. The passage towards the SE, which extends underneath the open-air theatre, is prone to collapse and has been secured with concrete pillars (Meier 2003; Konietzky *et al.* 2007; Mucke *et al.* 2008). Along the northwestern part of the known cave, the overburden above the cave is very thin, sometimes only a few metres. Residential buildings in this area are thus potentially in danger of collapse. An old sinkhole called Damloser Kuhle in the direction of the southeastern cave passages indicates a probable former extension of the cave system.

The evolution of the cave has been discussed in Kupetz & Brust (2008) and Ipsen & Mucke (2011), with its early evolution dating back to the last interglacial (*c.* 125 ka BP) as an active water-table cave along the 34.0–37.5 m a.s.l. level with autogenic recharge. When the palaeoclimate became colder and the Fennoscandian ice sheet approached the region, the supply of water stopped and the maze of enlarged cave passages was filled with glaciofluvial sediments. The infill blocked most of the formerly active passages and, since the Last Glacial Maximum (*c.* 21 ka BP), the reactivated infiltration of surface water has been efficiently blocked by sediments. Cave enlargement progressed under almost stagnant conditions, with typical solution forms (flat ceilings and steeply dipping side walls) developed along the 38–50 m a.s.l. level.

Gravity survey. Figure 4a projects the cave map (white outline) onto the topography and shows the locations of the three gravity profiles (red dots). The summit of the Kalkberg and the open-air theatre are marked as topographic features. The old sinkhole Damloser Kuhle is located south of the mapped cave passages. Some of the larger rooms – Zentralhalle, Barbarossahalle and Säulenhalle – are located in the transition zone from mechanically stable anhydrite to mechanically unstable gypsum, whereas some of the other rooms, such as the Gonzohalle, are entirely in the unstable gypsum.

Figure 4b shows the Bouguer gravity map (Δg_b). A value of 2200 kg m^{-3} has been chosen as the reference density and represents the average rock density for gypsum. With this choice, Bouguer gravity values below zero represent mass deficits relative to the gypsum rock and are thus possible voids and cave rooms. Note that the signal from the less dense salt is constant over the size of our working area as a result of the large extent of the salt dome

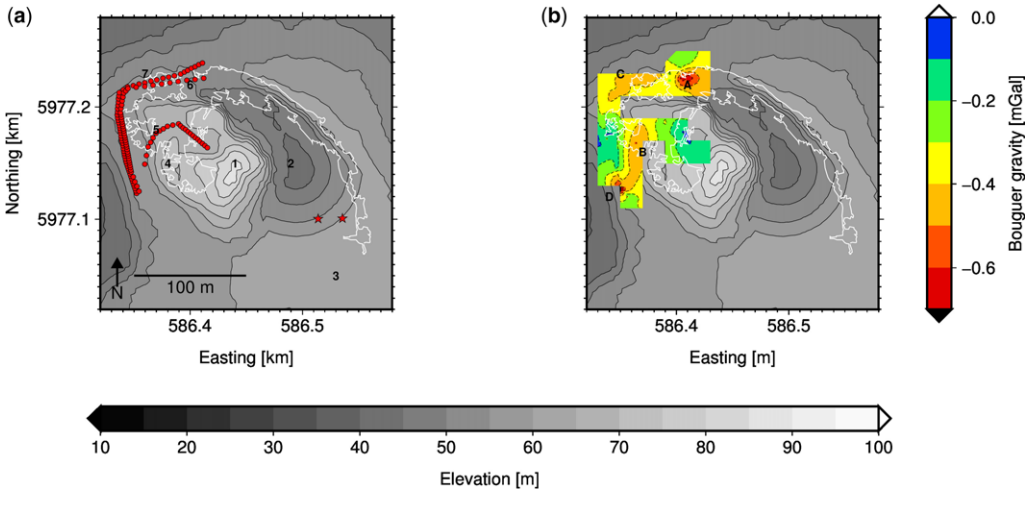

Fig. 4. Kalkberghöhle, Bad Segeberg, Schleswig-Holstein, Germany. (**a**) Location map showing gravity stations (red dots) and two former mining shafts (red stars). 1, Summit of the Kalkberg; 2, open-air theatre; 3, the old sinkhole Damloser Kuhl; 4, Zentralhalle; 5, Barbarossahalle; 6, Säulenhalle; 7, Gonzohalle. (**b**) Bouguer gravity map. A, Säulenhalle; B, Zentralhalle; C, Gonzohalle; D, artificial manhole on the road.

and is accounted for as a regional signal. The Bouguer gravity values are negative (−0.1 to −0.6 mGal) above the entire cave, indicating the karstified gypsum present underneath the gravity profiles. Three locations with a strong focused negative Bouguer gravity signal down to −0.6 mGal correspond to the rooms Säulenhalle, Zentralhalle and Gonzohalle. The Zentralhalle, however, has only been touched in its northern parts by the profile. Clearly the larger rooms dominate the Bouguer gravity signal, whereas the main cave level provides the broad negative background signal. The large gravity minimum in the far southwestern corner corresponds to the void of an artificial manhole on the road.

Jettenhöhle

The Jettenhöhle is located along the southern rim of the Harz Mountains (Fig. 5). The asymmetrical uplift of the Harz Mountains caused tilting of the soluble rocks of the Permian Zechstein period, which are exposed along the entire southern extension of the Harz Mountains and form a zone of intense karstification a few kilometres wide, with numerous caves, sinkholes and karst resurgences.

The area of interest, close to the city of Osterode and covering the karst regions Hainholz and Bollerkopf (Fig. 6), is characterized by hilly relief at elevations between 175 and 350 m a.s.l. Surface flow is only present in areas where the soluble Zechstein rocks are covered by insoluble marls and clays. Hydrologically, the region is subdivided into two catchments (Brandt *et al.* 1976). In the northwestern part, the Bollerkopfbach sinks into the active cave Marthahöhle. The Heiligentalbach, the remnant of an old valley coming from the Harz Mountains, with its headwaters lost by erosion, is a dry valley with an active surface creek still present in only a small portion, the continuation of which is unknown. The main drainage of the northwestern part is carried via the Schurfbach towards the Hackenbach creek and drains to the River Oder. In the southeastern

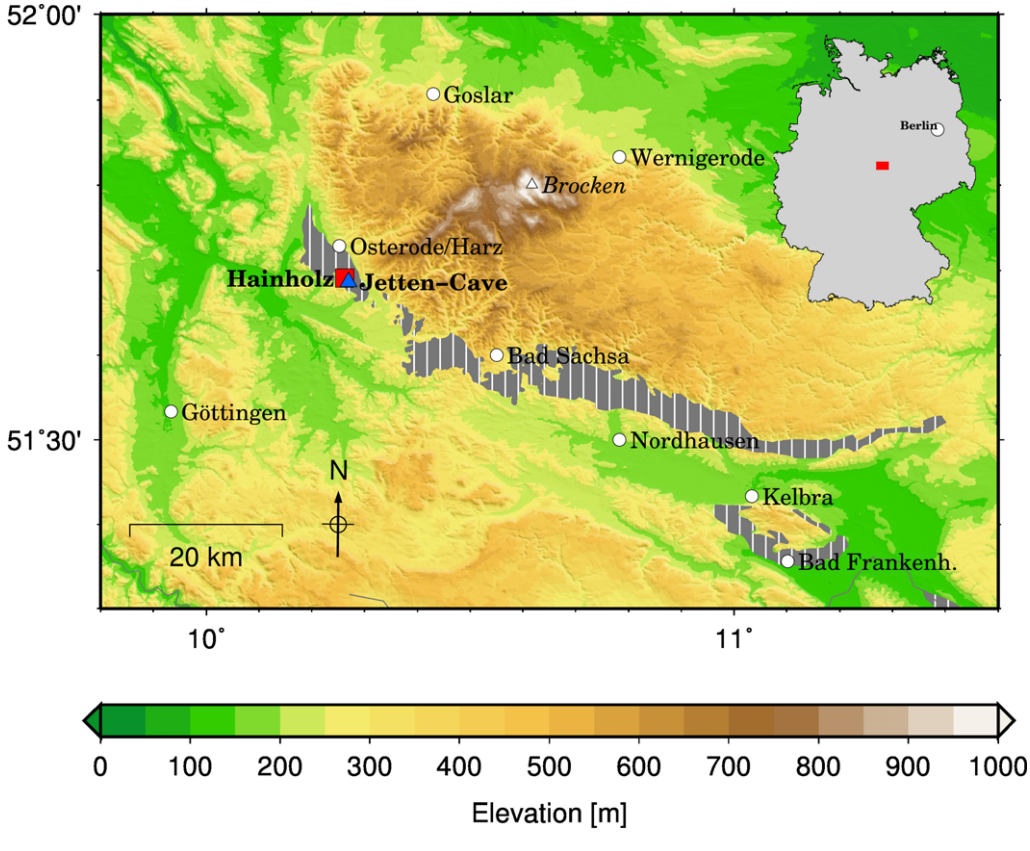

Fig. 5. Topographic map of the Harz Mountains showing the study site (red square) and cave (blue triangle), cities, geographical locations and outcrops of soluble Zechstein rocks in Lower Saxony, Thuringia and Saxony-Anhalt (grey hashed area). The inset shows the location (red square) of the figure within Germany.

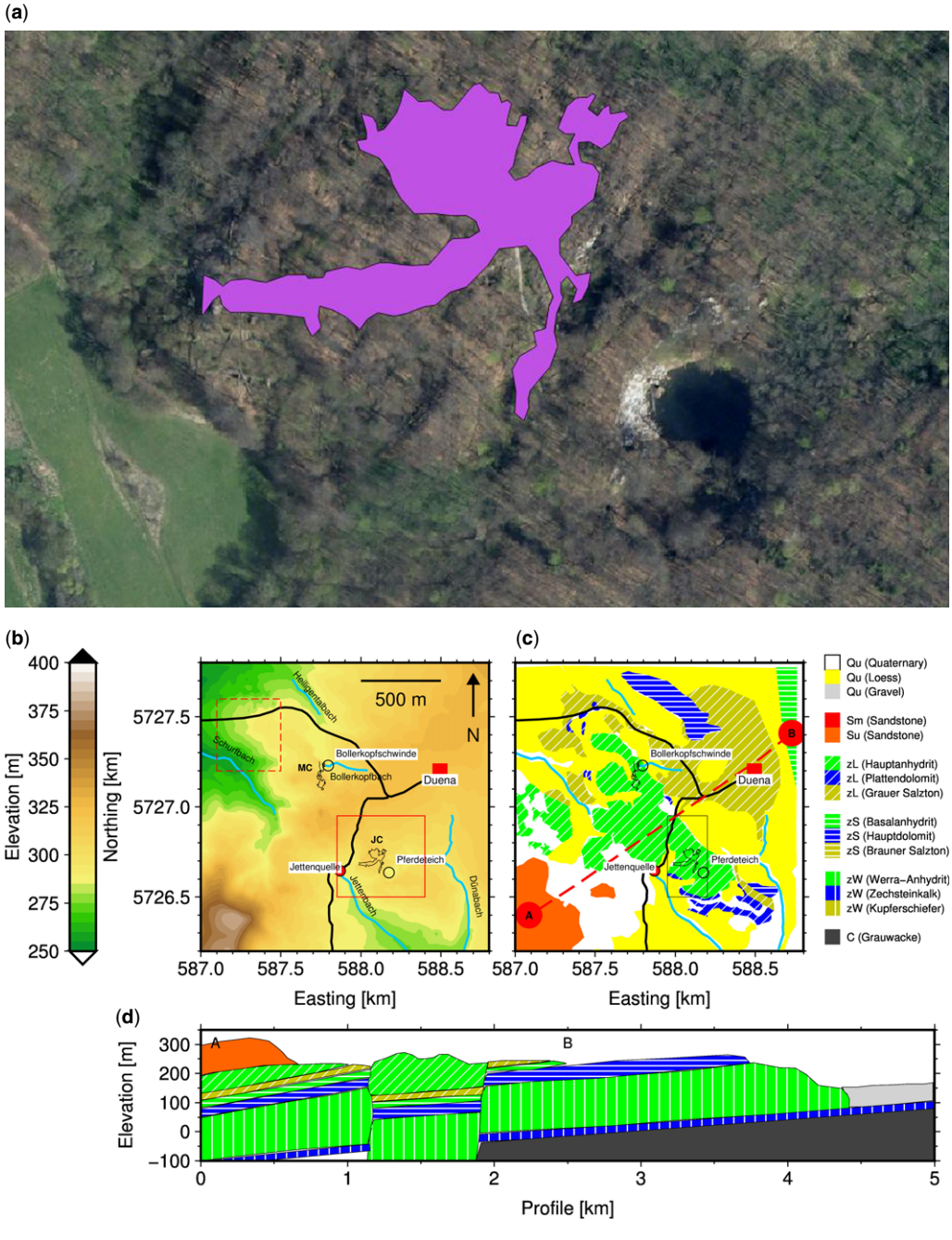

Fig. 6. Jettenhöhle, Osterode, Lower Saxony, Germany. (**a**) Map of the cave Jettenhöhle superimposed onto the digital ortho-photograph of the area. (**b**) Map view showing roads (solid black lines), rivers (solid light blue lines), sinkholes (open circles), springs (red closed circles), villages (red squares) and caves. JC, Jettencave; MC, Marthacave. The survey area is shown as a red solid rectangle. (**c**) Geological map showing lithological units. The location of the geological cross-section in part (d) is marked by the red dashed line. (**d**) Geological cross-section along profile shown in part (c).

part, the Düna Plateau is drained via the Dünabach creek, a subsurface drainage through the Jettenhöhle towards the Jettenbach creek and the Pferdeteich sinkhole, also draining towards the Jettenbach. The water from the Jettenbach flows to the River Sieber and also reaches the River Oder.

Three Zechstein sequences are exposed from north to south in the Hainholz/Bollerkopf area (Fig. 6) (e.g. Herrmann 1969, 1981*a*, *b*; Vladi 1972; Brandt *et al.* 1976; Jordan 1981; Kempe 1997, 2008). In the north, the sequence starts with the greywacke from the Paleozoic Harz Mountains. The Zechstein sequence follows, with z1/zW (Werra-Anhydrit) on top of the Paleozoic rocks, followed by z2/zS (Hauptdolomit, Basalanhydrit) and z3/zL (Grauer Salzton, Plattendolomit, Hauptanhydrit). Although the Werra-Anhydrit forms a prominent step, the zS sequence is barely visible. However, a tectonic graben structure has preserved large parts of the Hauptanhydrit of the zL sequence, which forms an extended and extremely karstified area. To the south, the Zechstein sequences are capped by Triassic Buntsandstein formations (mainly sandstone).

Our survey area was located in the graben structure with the zL sequence dominating the landscape. The Hauptanhydrit, with its shallow parts converted to gypsum from the surface towards the fluctuating water-table, is an extensively karstified area with deep karren, pits, numerous partially water-filled sinkholes and no significant surface runoff. The Plattendolomit exposed along the southwestern part of the Hainholz is characterized by a less rugged surface. Lithologically, the Plattendolomit is located below the Werra-Anhydrit, but the graben structure caused partial exposure due to bending of the rock layers.

The cave Jettenhöhle is located in the Hauptanhydrit (Fig. 7a). This cave, *c.* 748 m in total length (Kempe 1997, 2008), is developed in the gypsified

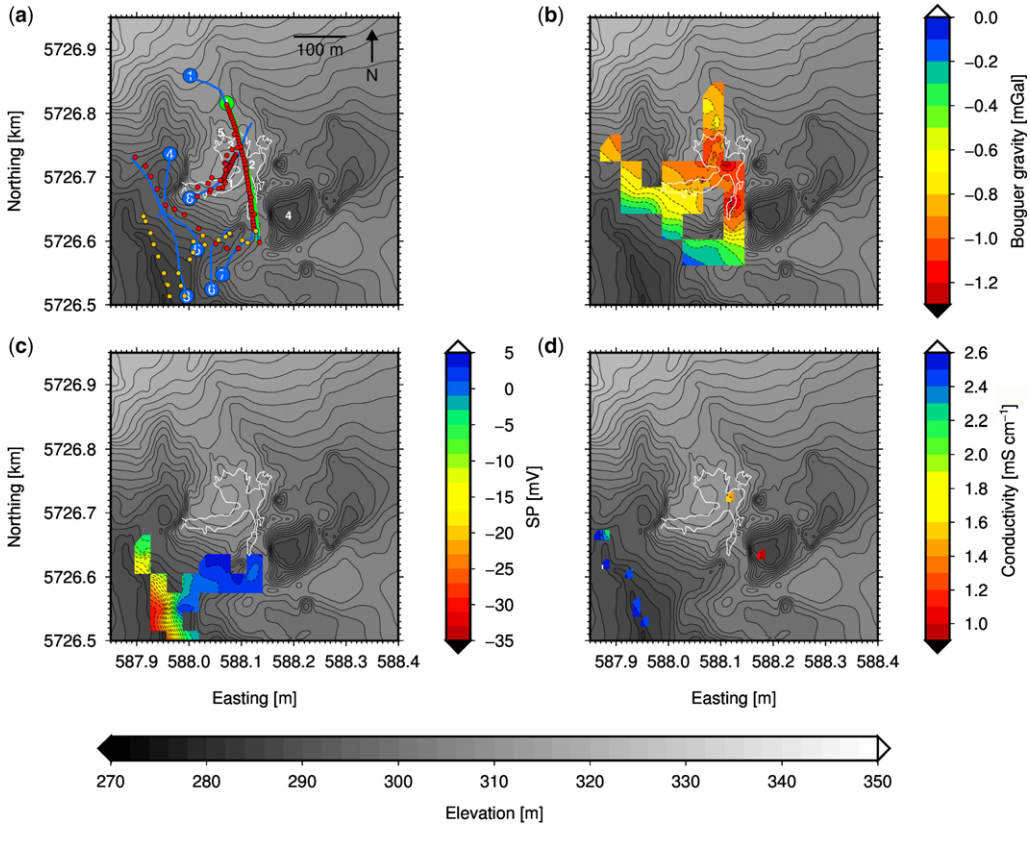

Fig. 7. Jettenhöhle, Osterode, Lower Saxony, Germany. (**a**) Location map with gravity stations (red dots), self-potential stations (yellow dots), electrical resistivity imaging profiles (blue lines with first electrode marked with profile number) and ground-penetration radar profile (green line). 1, Romarhalle; 2, Kreuzdom; 3, Jettenstube; 4, Pferdeteich collapse sinkhole; 5, Hirschzungenerdfall collapse sinkhole. (**b**) Bouguer gravity map. (**c**) Self-potential map. (**d**) Electrical conductivity map of open water.

part of the Hauptanhydrit. The cave consists of a large tunnel (Romarhalle), *c.* 10–20 m wide and several metres high, its deepest point being the large room Kreuzdom, 30 × 30 m wide and *c.* 13 m below the entrance. Two small lakes cover the Kreuzdom, about 1–2 m deep, but fluctuations in the lake level are small (10–20 cm on average). From the Kreuzdom, a large block pile leads to a further room, the Jettenstube, mostly filled with breakdown deposits and containing small lakes. All the cave lakes are a result of insoluble residuals from the dissolution of the gypsum (e.g. Kempe 2008), which cover the bottom parts of the cave and inhibit the water from totally disappearing. To the north of this room, a prominent collapse sinkhole (Hirschzungenerdfall) marks a former continuation of the cave. The Jettenhöhle has only a thin surface cover and collapse sinkholes mark older parts of the cave along the western and eastern sides. The large collapse sinkhole Pferdeteich is located to the east of the cave and receives water from the north, which disappears into a sink along the southern rim of the Pferdeteich (Hauptanhydrit). The lake in the Pferdeteich fluctuates substantially, with variations in the lake level of up to 7 m during the year.

We continue to obtain results from our geophysical surveys above and around the Jettenhöhle cave. We follow a strategy that picks up the signal from the cave and then use the knowledge gained from the surveys above the cave to extend our interpretation beyond the known cave passages into the surroundings.

The locations of all measurements are shown in Figure 7a. Gravity measurements were taken directly above the cave and in its vicinity. The station distances varied between 5 and 30 m. ERI measurements were made along seven profiles, mostly in the Wenner and Schlumberger set-up. Profiles 1 and 8 were located above the Jettenhöhle to track air-filled cave voids in the gypsum rock, whereas profiles 3–7 were located between the collapse sinkhole Pferdeteich and the creek Jettenbach. Depending on the length of the ERI profiles, 25 or 50 steel electrodes were used, with an electrode spacing between 4 and 5 m. ERI profile 1 was also explored with ground-penetrating radar measurements to obtain additional information on the cave voids. Self-potential measurements between the Pferdeteich and Jettenbach were carried out to shed light on the subsurface drainage of the Pferdeteich sinkhole. These measurements were complemented by electrical conductivity measurements in the sinkhole Pferdeteich, the lake in the Kreuzdom of the Jettenhöhle, the spring Jettenquelle and the Jettenbach.

Gravity survey. Figure 7b shows the Bouguer gravity map (Δg_b). A value of 2800 kg m^{-3} was chosen as the reference density, which represents the lower bound of the rock density for both the anhydrite and the dolomite. With this choice, Bouguer gravity values below zero represent mass deficits relative to the anhydrite/dolomite rock. Bouguer gravity values are negative (−0.3 to −0.5 mGal) above the entire cave, reflecting the less dense gypsum rock ($CaSO_4xH_2O$, density *c.* 2300 kg m^{-3}), which is a result of the hydration of the anhydrite ($CaSO_4$) within the groundwater zone. Cave rooms such as the Kreuzdom and Jettenstube are clearly visible by large negative Bouguer gravity values (−0.8 to −1.2 mGal). The large, sharply confined negative anomaly below −1.0 mGal is related to small breakdown passages in the south of the Kreuzdom, which are close to the surface and end on the side of a small collapse sinkhole (Kleine Jettenhöhle). Thus the cave voids have been clearly identified by gravity measurements. A second feature beyond the known cave limits is the regional trend in the Bouguer gravity data towards slightly positive values in the SW. The trend has a sharp gradient along the slopes of the valley of the creek Jettenbach. Comparing the Bouguer gravity data with the geological map (Fig. 6), we find a correlation of the gravity trend with the mapped outcrop of the Plattendolomit in the south. Our gravity data suggest that the denser dolomite extents even further north and limits the Werra-Anhydrit along the southern graben shoulder.

Electrical resistivity imaging. Figure 8 shows five ERI profiles above the cave Jettenhöhle. All the profiles have been carried out in the Wenner set-up, with 64 electrodes for profile 1 and 34 electrodes for profile 8. The electrical resistivity images ($\rho_{e,b}$), characterizing the bulk electrical resistivity of the rock were obtained from robust inversion with Res2DInv. They are both characterized by small root-mean-square values. Profile 1 is a 300 m long transect above the main cave rooms. Both rooms, the Jettenstube and the Kreuzdom, can be identified by resistivities >4000 Ω m, a value characteristic of air-filled voids. Although the Kreuzdom has an overburden of *c.* 10 m, the Jettenstube has been traversed at its northern end, where the overburden is already *c.* 15 m. The third high-resistivity anomaly, which is very pronounced, reflects the small passages in the southern part of the cave close to the small sinkhole. The gypsum rock itself is characterized by resistivities of *c.* 200–1000 Ω m. The low-resistivity anomaly (E) in the deeper section along the southern end of the profile, with values down to 20 Ω m, indicates flowing groundwater. Profile 8 is located above the main cave passages and the high-resistivity anomaly (D) at 15 m depth reflects the large cave passages Romarhalle and Jettenstube.

Profiles 3, 6 and 7 are all located south of the cave. In contrast with profiles 1 and 8, all three of these profiles are characterized by low resistivities

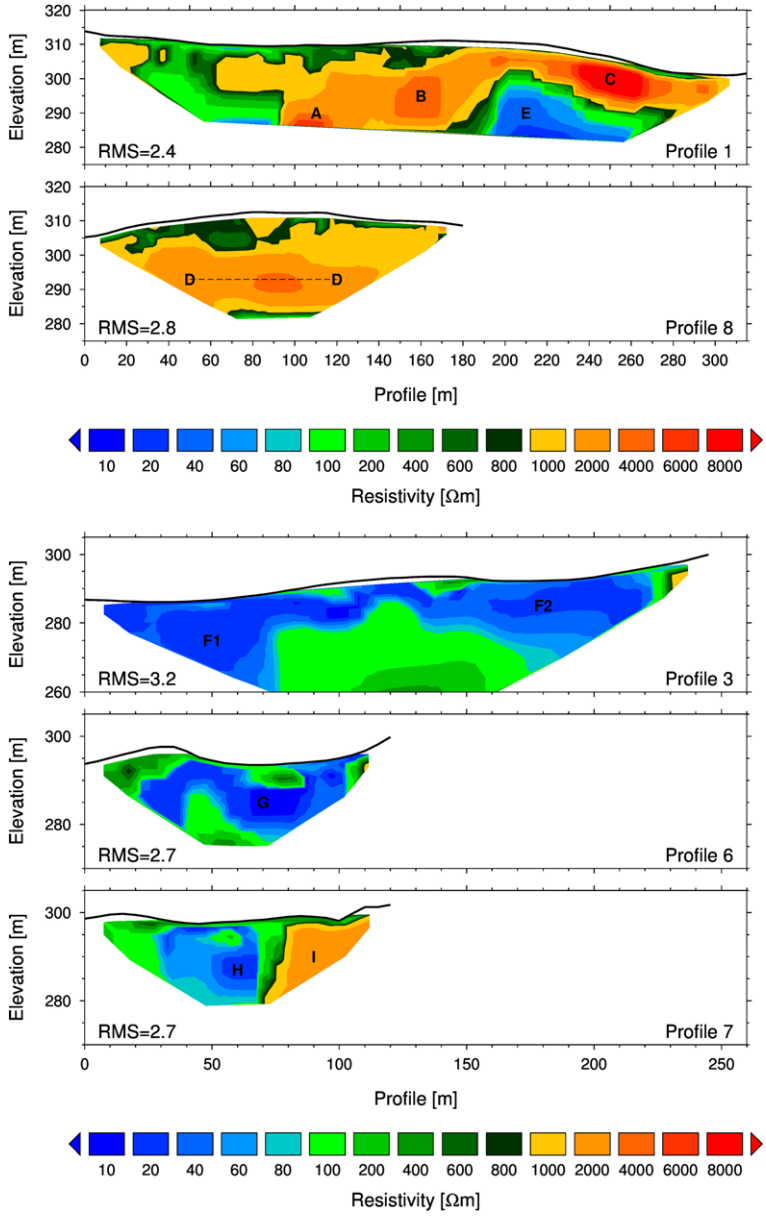

Fig. 8. Jettenhöhle, Osterode, Lower Saxony, Germany. Electrical resistivity imaging profiles 1, 8, 3, 6 and 7. A, Jettenstube; B, Kreuzdom; C, high-resistivity anomaly; D, large cave passages Romarhalle and Jettenstube; E, low-resistivity anomaly; F1, F2, G and H, low-resistivity anomalies; I, high-resistivity anomaly.

between 20 and 60 Ω m, indicating groundwater movement, and some patches with higher resistivities above 100 Ω m, possibly drier parts. The three low-resistivity parts (F1, G, H) are located along the same flow path and, together with anomaly E in profile 1, seem to map the subsurface drainage of the water from the collapse sinkhole Pferdeteich towards the creek Jettenbach. The sharp contrast between the low-resistivity (H) and the high-resistivity (I) parts in profile 7 marks the transition from gypsum to another rock type, which we interpret as Plattendolomit. We speculate that the Plattendolomit adjacent to the Werra-Anhydrit (converted to gypsum) is karstified, but to a lesser degree than

the gypsum. Therefore the gypsum drains surface water efficiently towards a lower phreatic zone, whereas the Plattendolomit, with its lower hydraulic conductivity, keeps the water coming from the Pferdeteich and thus reflects phreatic conditions with low electrical conductivities.

Electrical conductivity. Electrical conductivity measurements were taken in several open water bodies using a hand-held conductivity meter. Conductivities are automatically referenced to a temperature of 25°C. The measured electrical conductivity (Fig. 7d) increases from the input point to the karst aquifer, from the Pferdeteich (1.0 mS cm^{-1}), the small lake inside the Jettenhöhle (1.5 mS cm^{-1}), towards the Jettenquelle spring (2.2 mS cm^{-1}). We can compare these electrical conductivity readings ($\sigma_{e,f}$) measured in open water locations with the electrical resistivities ($\rho_{e,b}$) obtained from the ERI measurements. The electrical resistivity for the water samples is around $\rho_{e,b}$ = 4.5–10 Ω m, which is comparable with the low-resistivity values found in ERI profiles 3, 6 and 7 (20–40 Ω m). This is already a clear hint that the gypsum aquifer is strongly karstified (well-developed secondary porosity).

Self-potential. Self-potential measurements were carried out with non-polarizable copper–copper sulphate electrodes and a multimeter along the small valley between the Pferdeteich collapse sinkhole and the local base level Jettenbach. The self-potential measurements were referenced to a base electrode located on the rim of the sinkhole in the vadose zone. The mapped self-potential measurements are shown in Figure 7c. The self-potential is around the zero reference value along the higher parts of the valley and decreases to negative values downstream, with a final strong gradient along the banks of the Jettenbach creek to values below −30 mV. Both the amplitude and the pattern are indicative of a self-potential induced by groundwater flow, thus it is likely that the water disappearing into the Pferdeteich sinkhole reappears along the Jettenbach creek.

Structural models

We assembled three-dimensional structural models of the subsurface for both cave sites based on our geophysical data and information about the local and regional geological setting. We built a three-dimensional structural model of the cave sites and their surroundings within the PREDICTOR software package (e.g. Kaufmann *et al.* 2012, 2015*a*, *b*). The PREDICTOR package uses a given digital topography, which is extended to depth with different lithological layers. Each layer can have different physical properties and can accommodate three-dimensional structures such as caves, voids or other objects. This numerical model is then used to predict different geophysical signals. The program basically performs the calculations in three parts: (1) the assembly of the model; (2) the solution of the governing equations; and (3) the prediction of geophysical signals. Details can be found in Kaufmann *et al.* (2015*a*).

The model is discretized in three spatial dimensions and then boundary conditions are set for the hydraulic problem (recharge as fixed flow, resurgences as fixed head). The groundwater equation is then solved as a transient, three-dimensional problem for both laminar and turbulent flow, thus appropriately describing the flow in porous, fractured rocks. To predict the gravity signal (used in this work), we used the discretized parallelepipedal elements to predict a Bouguer gravity signal for each block and then added all the block contributions to obtain a large-scale signal.

Kalkberghöhle

We used a digital elevation model with 5 m resolution for the Kalkberghöhle in Bad Segeberg in northern Germany. The subsurface structure was defined as gypsum. We neglected the anhydrite core of the structure, but as our gravity readings had only been taken above the gypsified part of the cave, our simplification was acceptable. The underlying salt diapir was a regional structure in our model, thus it affected the total gravity signal by the lower mass of the salt, but with no lateral variation on our scale. The structural model is shown in Figure 9a, with the cave Kalkberghöhle in dark red and the Bouguer gravity data as colour-coded squares on top.

The cave void has been discretized from the map of Fricke (1990). As the ceiling height of some of the cave rooms – such as the Zentralhalle, Barbarossahalle, Säulenhalle and Gonzohalle – has only been measured locally, we extended the room height to satisfy our gravity measurements.

The reason for the extension of the mapped cave passages towards the surface can be seen in Figure 9b, where we compare the observed and predicted Bouguer anomalies above the western part of the Kalkberghöhle. We can satisfactorily predict both the broad negative anomaly above the entire cave, representing the highly karstified gypsum, and the three local minima above the larger cave rooms, which seem to extend close to the surface, as our prediction suggests.

Jettenhöhle

We used a digital elevation model with 5 m resolution for the Hainholz area in the southern Harz Mountains and defined two lithological units, the Hauptanhydrit and the Plattendolomit below.

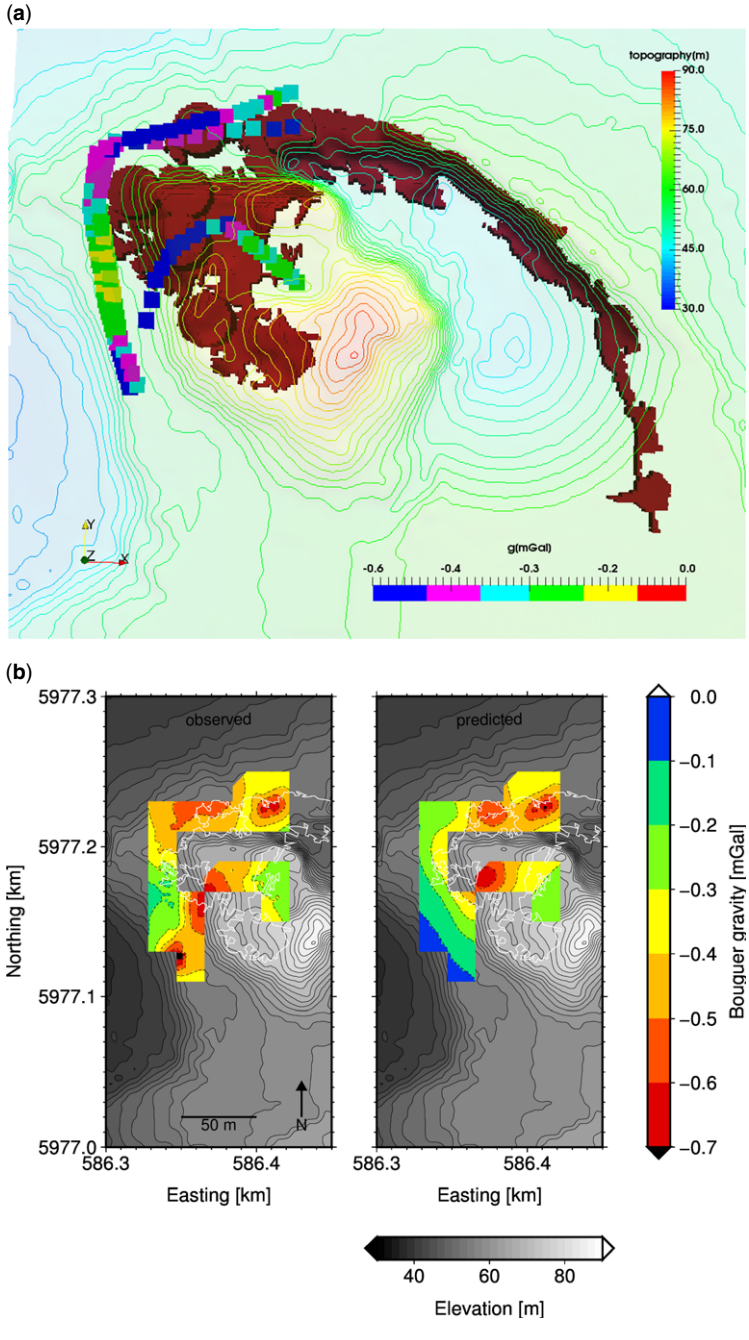

Fig. 9. Kalkberghöhle, Bad Segeberg, Schleswig-Holstein, Germany. (**a**) Topographic contour map showing the Kalkberghöhle cave as a dark red block, gravity profiles as map. (**b**) Observed and modelled Bouguer gravity anomaly over the area.

A structural model of this set-up is shown in Figure 10a. Here the Jettenhöhle is shown in dark red, the topography as colour-coded contours and the ERI profiles as cross-sections. The Pferdeteich sinkhole is the large depression at the front and the valley in the upper left is the Jettenbach creek.

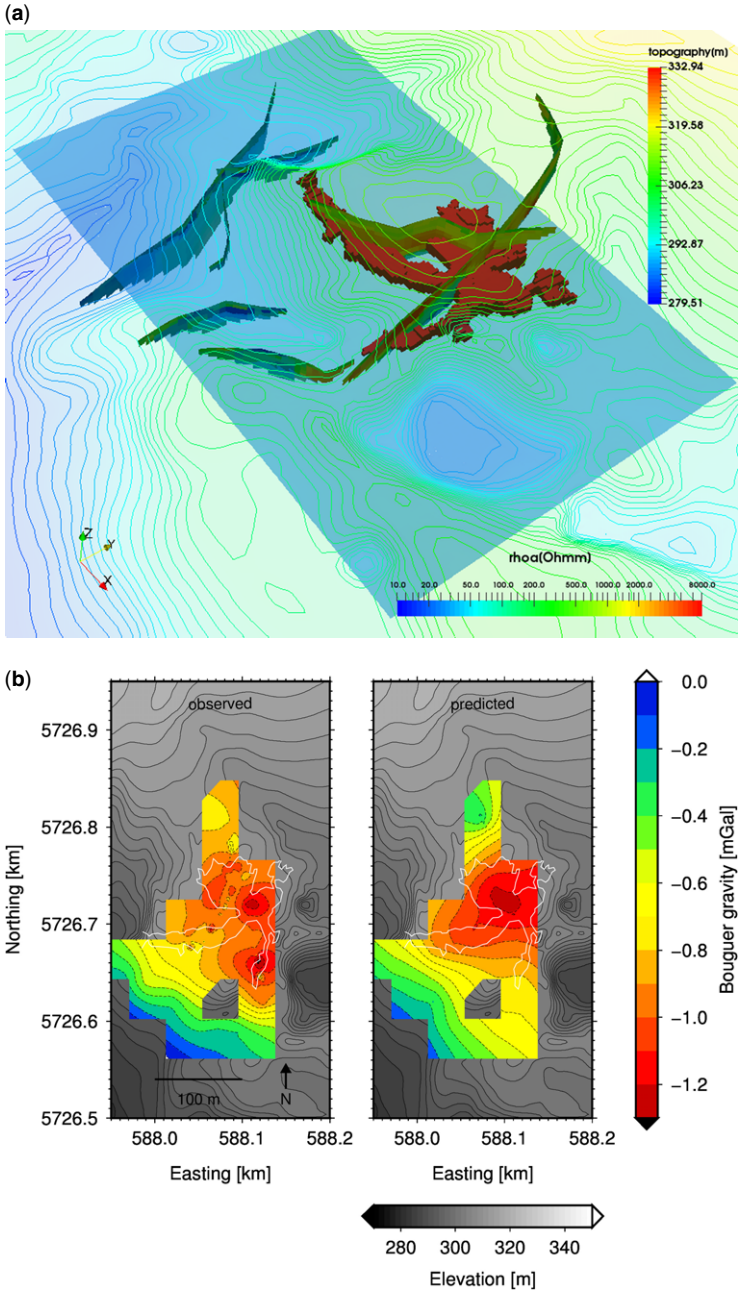

Fig. 10. Jettenhöhle, Osterode, Lower Saxony, Germany. (**a**) Topographic contour map showing the Jettenhöhle cave as a dark red block and electrical resistivity imaging profiles as cross-sections. (**b**) Observed and modelled Bouguer gravity anomaly over the area.

We used this structural model to predict the Bouguer anomaly of the area (Fig. 11). Our model prediction can explain the strong negative signal (down to −1.2 mGal) caused by the larger cave voids. The small passages to the south, which cause a strong local negative Bouguer signal, are not

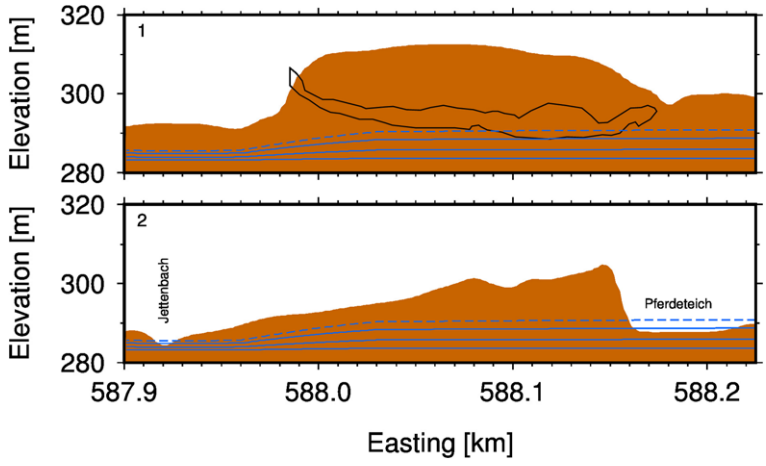

Fig. 11. Jettenhöhle, Osterode, Lower Saxony, Germany. Two cross-sections along the axis Jettenbach-Pferdeteich (2, bottom) and the Jettenhöhle (1, top). Topography in brown, cave cross-section as black line, and three water table models (blue solid lines) for 0, 5 and 10 mm/day recharge, and a higher water table (dashed blue line) for 15 mm/day recharge.

captured as a result of the limited resolution of the structural model. In addition to the local Bouguer signal, the regional trend towards larger values close to the Jettenbach creek is also modelled satisfactorily. The amplitude of this regional signal is slightly underestimated, which was probably caused by the limited information on the geological map (Fig. 6) about the outcrop of the Plattendolomit, which is partially covered by loess in this area.

We add a transient three-dimensional groundwater flow model, modelled on a daily basis with recharge by precipitation (up to 15 mm day^{-1}) and flow towards the local base level Jettenbach. The subsurface consists of gypsum (hydraulic conductivity $K_f = 10^{-4}$ m s^{-1}, specific storage $S_s = 5 \times 10^{-6}$ 1 m^{-1}), dolomite ($K_f = 10^{-7}$ m s^{-1}, $S_s = 5 \times 10^{-7}$ 1 m^{-1}) and the cave void. The resulting water-table gently dips towards the creek Jettenbach, with a distinct gradient along the transition from gypsum to dolomite. ERI profiles 3, 6 and 7, and, in part, profile 1, show low electrical resistivity in the phreatic zone below the water-table; ERI profiles 1 and 8 show high electrical resistivity around the cave voids in the vadose zone. Thus the groundwater flow explains the mapped ERI measurements. The low hydraulic conductivity of the dolomite is responsible for keeping the water-table high after substantial rain, with possible back-flooding of the Pferdeteich sinkhole. This is often observed after snowmelt in spring, with levels rising by 2–4 m, as can be seen in the two cross-sections below the structural model.

The water-table may rise even higher during stronger recharge events and flood the lower part of the cave, as can be seen in the two cross-sections between Pferdeteich–Jettenbach and along the Jettenhöhle (Fig. 11b, dashed blue line). This rare flooding of the cave has been documented (Vladi 1972).

Conclusions

We have compiled a large dataset of geophysical surveys in and above the Kalkberghöhle and Jettenhöhle caves, developed in the Hauptanhydrit formation of the z3 (Leine) sequence of Permian Zechstein rocks. We chose these two cave sites because the caves have a shallow overburden of 10–40 m and are characterized by small passages and large rooms. With these favourable settings, we expect the caves to be detectable by indirect geophysical measurements.

We have shown that the known and surveyed cave passages can be traced with both gravity and ERI measurements, which reflect the lower density and the different electrical resistivities of the cave voids and host rock. Gravity is a useful method here as we can identify the cave voids in the Bouguer gravity signal as local negative anomalies and the geological setting as a regional trend in the Bouguer gravity data. The ERI measurements, mostly carried out in the Wenner set-up, provide additional information about the subsurface geology and water content, which are useful in characterizing the hydrological situation. Other ERI set-ups, such as the Schlumberger or dipole–dipole set-ups, essentially confirmed our results, with the latter set-up being less useful due to the poor signal-to-noise ratio.

For the Kalkberghöhle locality, we were able to explain large parts of the Bouguer gravity signal of the cave void using a numerical prediction of the digitized cave map. We were able to address the ceiling heights in the larger rooms, which have not been accurately mapped in the field.

For the locality Hainholz in the southern Harz Mountains, we have shown that, in addition to the strong negative Bouguer data above the cave, a regional trend towards larger Bouguer values is observed in the western direction. This increase in gravity indicates the denser Plattendolomit partly outcropping along the western edge of the graben structure. Observations of lake level fluctuations then enabled us to propose a simple hydrogeological model of the Hainholz area.

The geophysical surveys were part of the BSc theses of Alexandra Werner and Johann Diezel, supervised by GK. Field support from Ron Freibothe, Julio Galindo-Guerreros, Thomas Hiller, Grit Jahn, Lucinda Gürlich, Johannes Mayr, Douchko Romanov and Alexandra Werner is greatly acknowledged. This work was funded by the Deutsche Forschungsgemeinschaft under research grant KA1723/6.

References

Bechtel, T.D., Bosch, F.P. & Gurk, M. 2007. Geophysical methods. *In*: Goldscheider, N. & Drew, D. (eds) *Methods in Karst Hydrogeology*. Balkema, Rotterdam, 171–199.

Brandt, A., Kempe, S., Seeger, M., Vladi, F. 1976. Geochemie, Hydrographie und Morphogenese des Gipskarstgebietes von Düna/Südharz. *Geologisches Jahrbuch Reihe C*, **15**, 3–55.

Butler, D. 1984. Microgravimetric and gravity-gradient techniques for detection of subsurface cavities. *Geophysics*, **49**, 1084–1096.

Carbonel, D., Gutiérrez, F. *et al.* 2013. Differentiating between gravitational and tectonic faults by means of geomorphological mapping, trenching and geophysical surveys. The case of Zenzano Fault (Iberian Chain, N Spain). *Geomorphology*, **189**, 93–108.

Carbonel, D., Rodríguez, V. *et al.* 2014. Evaluation of trenching, ground penetrating radar (GPR) and electrical resistivity tomography (ERT) for sinkhole characterization. *Earth Surface Processes and Landforms*, **39**, 214–227.

De Waele, J., Gutierrez, F., Parise, M. & Plan, L. 2011. Geomorphology and natural hazards in karst areas: a review. *Geomorphology*, **134**, 1–8.

Dobecki, T.L. & Upchurch, S. 2006. Geophysical applications to detect sinkholes and ground subsidence. *The Leading Edge*, **25**, 336–341.

El-Qady, G., Hafez, M., Abdalla, M. & Ushijima, K. 2005. Imaging subsurface cavities using geoelectric tomography and ground-penetrating radar. *Journal of Cave & Karst Studies*, **67**, 174–181.

Ford, D.C. & Williams, P.W. 2007. *Karst Geomorphology and Hydrology*. Wiley, Chichester.

Fricke, U. 1990. Ein neuer Plan der Segeberger Kalkberghöhle. *Mitteilungen des Verbandes der Deutschen Höhlen- und Karstforscher*, **36**, 77–85.

Gutiérrez, F. 2010. Hazards associated with karst. *In*: Alcántara, I. & Goudie, A. (eds) *Geomorphological Hazards and Disaster Prevention*. Cambridge University Press, Cambridge, 161–175.

Gutiérrez, F., Parise, M., De Waele, J. & Jourde, H. 2014. A review on natural and human-induced geohazards and impacts in karst. *Earth Science Reviews*, **138**, 61–88.

Herrmann, A. 1969. Einführung in die Geologie, Morphologie und Hydrogeologie des Gipskarstgebietes am südwestlichen Harzrand. *In*: Herrmann, A. & Pfeiffer, D. (eds) *Der Südharz – seine Geologie, seine Höhlen und Karsterscheinungen*. Verband der deutschen Höhlen- und Karstforscher, **9**, 1–10.

Herrmann, A. 1981*a*. Eine neue geologische Karte des Hainholzes bei Düna/Osterode am Harz. *Berichte der Naturhistorischen Gesellschaft Hannover*, **124**, 17–33.

Herrmann, A. 1981*b*. Zum Gipskarst am südwestlichen und südlichen Harzrand. *Berichte der Naturhistorischen Gesellschaft Hannover*, **124**, 35–45.

Ipsen, A. & Mucke, D. 2011. *Die Segeberger Höhle – eine Welt im Verborgenen*. Fledermaus-Zentrum, Bad Segeberg.

Jarvis, A., Reuter, H., Nelson, A. & Guevara, E. 2008. Hole-filled Seamless SRTM Data V4. International Centre for Tropical Agriculture, http://srtm.csi.cgiar.org

Jordan, H. 1981. Karstmorphologische Kartierung des Hainholzes (Südharz). *Berichte der Naturhistorischen Gesellschaft Hannover*, **124**, 47–53.

Kardel, J., Mucke, D. & Frühwirt, T. 2009. Felssicherung in Anhydrit und Gips am Beispiel des Kalkbergstadions Bad Segberg (Rock stabilization of anhydrite and gypsum by the example of the Kalkbergstation Bad Segeberg). *In*: *VerÃ¶ffentlichungen 17*. Tagung für Ingenieurgeologie und Forum Junge Ingenieurgeologen, 6–9 May 2009, Horchschule Zittau/Görlitz, 149–154.

Kaufmann, G. 2014. Geophysical mapping of solution and collapse sinkholes. *Journal of Applied Geophysics*, **111**, 271–288.

Kaufmann, G. & Romanov, D. 2016. Structure and evolution of collapse sinkholes: combined interpretation from physico-chemical modelling and geophysical field work. *Journal of Hydrology*, **540**, 688–698.

Kaufmann, G., Jahn, G., Galindo-Guerreros, J. & Nielbock, R. 2012. Geophysical exploration of cave sites: the case of the Unicorn Cave, Scharzfeld/Harz, Germany. *Braunschweiger Naturkundliche Schriften*, **11**, 69–80.

Kaufmann, G., Ullrich, B. & Hoelzmann, P. 2015*a*. Two iron-age settlement sites in Germany: from field work via numerical modelling towards an improved interpretation. *Archaeological Discovery*, **3**, 1–14.

Kaufmann, G., Nielbock, R. & Romanov, D. 2015*b*. The Unicorn Cave, Southern Harz Mountains, Germany: from known passages to unknown extensions with the help of geophysical surveys. *Journal of Applied Geophysics*, **123**, 123–140.

Kempe, S. 1997. Gypsum karst of Germany. *International Journal of Speleology*, **25**, 209–224.

KEMPE, S. 2008. Gipskarst – ein Überblick. *Exkursionsführer und Veröffentlichung der Deutschen Gesellschaft für Geowissenschaften*, **235**, 30–41.

KONIETZKY, H., WALTER, K. & FRÜHWIRT, T. 2007. *Standsicherheitsgutachten Kalkberghöhle Bad Segeberg*. Unpublished report, Geomontan GmbH.

KUPETZ, M. & BRUST, M. 2008. Neue Beobachtungen in der Segeberge Kalkberghöhle – Gerinnehöhlen-Stockwerk, Eiskeil-Pseudomorphose und Fazetten. *Mitteilungen des Verbandes der deutschen Höhlen- und Karstforscher*, **54**, 76–84.

LOKE, M. & BARKER, R. 1995. Rapid least-squares inversion of apparent resistivity pseudosections using a quasi-Newton method. *Geophysical Prospecting*, **44**, 131–152.

LOKE, M.H. & BARKER, R.D. 1996. Practical techniques for 3D resistivity surveys and data inversion. *Geophysical Prospecting*, **44**, 499–523.

MARGIOTTA, S., NEGRI, S., PARISE, M. & VALLONI, R. 2012. Mapping the susceptibility to sinkholes in coastal areas, based on stratigraphy, geomorphology and geophysics. *Natural Hazards*, **62**, 657–676.

MARGIOTTA, S., NEGRI, S., PARISE, M. & QUARTA, T.A.M. 2016. Karst geosites at risk of collapse: the sinkholes at Nociglia (Apulia, SE Italy). *Environmental Earth Sciences*, **75**, 1–10.

MEIER, G. 2003. Ingenieurgeologische Ergebnisse bei der Standsicherungsanalyse der Kalkberghöhle in Bad Segeberg. *In*: *Veröffentichungen 14*. Tagung für Ingenieurgeologie, CAU Kiel, 353–358.

MOCHALES, T., CASAS, A.M., PUEYO, O., ROMAN, M.T., POCOVI, A., SORIANO, M.A. & ANSON, D. 2008. Detection of underground cavities by combining gravity, magnetic and ground penetrating radar surveys: a case study from the Zaragosa area, NE Spain. *Environmental Geology*, **53**, 1067–1077.

MUCKE, D., RAHMEL, U., DENSE, C., GLOZA-RAUSCH, F., IPSEN, A., VÖLKER, C. & VÖLKER, R. 2008. Vertretbare Eingriffe im Segeberger Karst in Ausführung. *Mitteilungen des Verbandes der deutschen Höhlen- und Karstforscher*, **54**, 68–75.

PALMER, A. 2007. *Cave Geology*. Cave Books, Dayton, OH.

PARISE, M. & LOLLINO, P. 2011. A preliminary analysis of failure mechanisms in karst and man-made underground caves in Southern Italy. *Geomorphology*, **134**, 132–143.

ROSS, P.-H. 1990. Die Tektonik der Segeberger Höhle. *Mitteilungen des Verbandes der deutschen Höhlen- und Karstforscher*, **36**, 29–32.

ROSS, P.-H. 1993. Die Segeberger Karstlandschaft. *Berichte aus dem Geologischen Landesamt Schleswig-Holstein*, **2**, 33–48.

SPARR, H.-P. 1997. *Der Kalkberg: Naturdenkmal und Wahrzeichen der Stadt Bad Segeberg*. Christinas, Hamburg.

TELFORD, W.M., GELDART, L.P. & SHERIFF, R.E. 2012. *Applied Geophysics*. 2nd edn. Cambridge University Press, Cambridge.

VLADI, F. 1972. Verkarstung und Höhlenentwicklung im Gips. *In*: KEMPE, S., MATTERN, E., REINBOTH, F., SEEGER, M. & VLADI, F. (eds) *Die Jettenhöhle bei Düna und ihre Umgebung Abh*. Karst- und Höhlenkunde A6, Verband der deutschen Höhlen- und Karstforscher, Munich, Germany.

WENZEL, F. 1996. The nanogal software: Earth tide data processing package eterna 3.30. *Bulletin d'Informations Marees Terrestres*, **124**, 9425–9439.